Front. Electr. Electron. Eng. 2012, 7(4): 467–476
DOI 10.1007/s11460-012-0210-2

RESEARCH ARTICLE

A. DEENADAYALAN, Chintala DHANANJAI, G. SARAVANA ILANGO

Modified sliding mode observer for wide speed range operation of brushless DC motor

Abstract This paper describes an adaptive gain sliding mode observer for brushless DC motor for large variations in speed. Sensorless brushless DC motor based on sliding mode observer exhibits multiple zero crossing in back electromotive force (EMF) which leads to commutation problems at low speed. In this paper, a modified sliding mode observer incorporating a speed component in the estimation of back EMF is proposed. It is found that after incorporating the speed component in the back EMF observer gain, multiple zero crossings at low speeds and phase shift at higher speeds are eliminated. The trapezoidal back EMF observer is implemented experimentally on a digital signal processor (DSP) board. The effectiveness of the proposed method is demonstrated through simulations and experiments.

Keywords brushless DC (BLDC), back electromotive force (EMF), sliding mode observer

1 Introduction

Brushless DC (BLDC) motor, also called permanent magnet (PM) DC synchronous motor, is one of the motor types that have gained popularity rapidly, mainly because of its high power density, reliability, efficiency, maintenance free nature, and silent operation [1]. It is widely used in a variety of applications such as industrial automation, computers, aerospace [2], military (gun turrets drives for combat vehicles) and household products. For BLDC motors, a constant supply of position information is necessary; thus, a position sensor with high resolution, such as a shaft encoder or a resolver, is typically used [3]. However, this increases the cost and size of the motor, and a special arrangement needs to be made for mounting the sensors. Low-cost Hall-effect sensors are commonly used because only the knowledge of six commutation instants per electrical cycle is needed. However, Hall sensors are temperature sensitive and hence the operation of the motor is limited, which could reduce the system reliability. Furthermore, it is tedious to install and maintain a position sensor due to the limited assembly space and rigid working environment with severe vibrations and high temperature. Therefore, various position-sensorless control schemes have been developed using low cost microprocessors and digital signal processors.

Generally, the current commutation point of the BLDC motor is estimated by the zero crossing of the back electromotive force (EMF) [4]. The conventional scheme needs the motor neutral point voltage to get the zero crossing of the back EMF [5,6]. Virtual neutral point is created using wye connected resistive circuit. However, this neutral point is not stable during pulse width modulation (PWM) switching. Mostly low pass filters which introduce delay are used to eliminate the higher order harmonics [4]. Another method [7,8] compares the back EMF voltage with respect to the negative DC bus potential. Detecting the conduction of free-wheeling diode in the open phase also gives the zero-crossing point of the back EMF waveform [9]. However, the circuit becomes complex due to the requirement of six additional power supplies. A few other schemes, such as back EMF integration, using third harmonic voltage were also developed. In back EMF integration method [10–12], integration starts from zero crossing of the back EMF and stops when the threshold value is reached, which gives the commutation instant. This approach has the advantage of reduced switching noise sensitivity and automatic adjustments of the inverter switching instants to changes in the rotor speed. A low-cost sensorless scheme has been proposed [13] using one terminal voltage. Based on this technique, due to the interpolation of the switching instants

Received September 4, 2012; accepted September 23, 2012

A. DEENADAYALAN (✉), Chintala DHANANJAI,
G. SARAVANA ILANGO
Power Converters Research Laboratory, Department of Electrical and Electronics Engineering, National Institute of Technology Tiruchirappalli, Tamilnadu, India
E-mail: dayalanbe@gmail.com

for other two phases from the sensed phase switching instants, frequent, rapid acceleration, or deceleration is not possible. The rotor position is determined based on the stator third harmonic voltage component which is the sum of the terminal voltages [14–16]. All the above mentioned schemes work well only over a limited range of speed.

Observer principles have been applied to sensorless operation of PM machines to suit wide range of speeds [17]. A machine and power converter are supplied with one or more inputs (e.g., voltages) and produce several measured outputs (e.g., currents). A mathematical model of the machine combination is supplied with the same inputs and produces estimates of the outputs. These estimated outputs are compared with the measured outputs to yield an estimation error, which is fed back to the model to assist in correcting the estimates. If the estimation error is small, the model replicates the behavior of the real converter and machine. An extended Kalman filter estimator for a brushless DC motor has been developed [18,19]. However, system identification and state estimation require complex computations and sensitive to noise.

Sliding mode observers have attractive advantages of robustness to disturbances and low sensitivity to parameter variation [20,21]. Sliding mode observer is designed based on the dynamic equations to estimate the induced back EMF, rotor position, and speed of the BLDC motor [22–25]. The back EMF information was obtained from the filtered switching signals relative to current estimation error. In Ref. [22], NSGA II algorithm was applied to select the gain of the sliding mode observer.

However, in all the methods observer gain is maintained as a fixed value as given in Refs. [23,24] for estimating back EMF which suits well only for particular range of speeds for which it is designed. The invariable observer gain produces multiple zero crossings for low speeds and a phase delay for large range of speeds. In the proposed method, the value of the observer gain varies in accordance with the variation of speed to match the estimated back EMF with actual back EMF. The proposed sliding mode observer was implemented experimentally on a digital signal processor (DSP) TMS320LF2407A board. The good correlation between the simulation and experimental results establish the validity of the proposed method.

The paper is organized as follows. In Section 2, a BLDC motor model is presented. In Section 3, the proposed modified sliding mode observer scheme for BLDC motor is explained. Further, the details of the experimentation and results are presented in Section 4.

2 BLDC motor model

A BLDC motor with trapezoidal back EMF coefficient is taken into consideration. The equivalent circuit of BLDC motor with three-phase six-switch inverter is shown in Fig. 1. The BLDC motor can be modeled using the following equations considering that the phase voltages are balanced:

$$\frac{\mathrm{d}}{\mathrm{d}t}(i_a - i_b) = -\frac{R}{L}(i_a - i_b) - \frac{1}{L}E_{ab} + \frac{1}{L}V_{ab},$$

$$\frac{\mathrm{d}}{\mathrm{d}t}(i_b - i_c) = -\frac{R}{L}(i_b - i_c) - \frac{1}{L}E_{bc} + \frac{1}{L}V_{bc},$$

$$\frac{\mathrm{d}}{\mathrm{d}t}(i_c - i_a) = -\frac{R}{L}(i_c - i_a) - \frac{1}{L}E_{ca} + \frac{1}{L}V_{ca}, \qquad (1)$$

where R and L are the resistance and inductance of the BLDC motor, respectively. (E_{ab}, E_{bc}, E_{ca}) are the line back EMF, (V_{ab}, V_{bc}, V_{ca}) are line voltages of the inverter, and (i_a, i_b, i_c) are the phase currents. If the sampling period is significantly less than the electrical and mechanical time constants then the back EMF can be assumed to be constant during each sampling period [24] and hence differentiation of the back EMF equals zero. Thus, Eq. (1) is written as

$$\frac{\mathrm{d}}{\mathrm{d}t}(i_a - i_b) = -\frac{R}{L}(i_a - i_b) - \frac{1}{L}E_{ab} + \frac{1}{L}V_{ab},$$

$$\frac{\mathrm{d}}{\mathrm{d}t}(i_b - i_c) = -\frac{R}{L}(i_b - i_c) - \frac{1}{L}E_{bc} + \frac{1}{L}V_{bc},$$

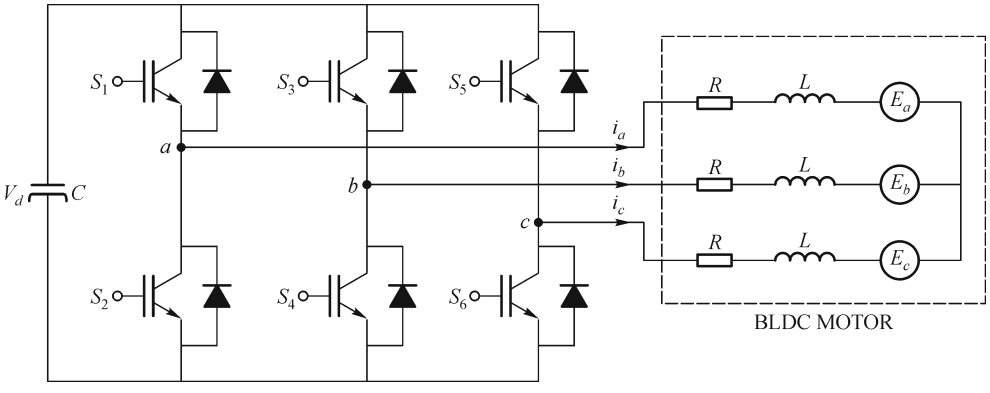

Fig. 1 BLDC motor drive with inverter

$$\frac{\mathrm{d}}{\mathrm{d}t}E_{ab} = 0,$$

$$\frac{\mathrm{d}}{\mathrm{d}t}E_{bc} = 0. \tag{2}$$

3 Design of the proposed sliding mode observer for BLDC motor

The system shown in Eq. (2) depends mainly upon the line currents and line voltages. Conventional sliding mode observer that estimates back EMF is shown in Fig. 2 where the back EMF observer gain is maintained as constant. Equation (2) is transformed into sliding mode observer as mentioned in Ref. [24], which restricts the motor operation to a particular range of speed. Hence, it is modified by including a function of speed in back EMF observer gain to operate for all range of speeds and is given by

$$\dot{\hat{x}}_1 = -\frac{R}{L}x_1 - \frac{1}{L}\hat{x}_3 + \frac{1}{L}V_{ab} + K_{11}\mathrm{sign}(x_1 - \hat{x}_1),$$

$$\dot{\hat{x}}_2 = -\frac{R}{L}x_2 - \frac{1}{L}\hat{x}_4 + \frac{1}{L}V_{bc} + K_{22}\mathrm{sign}(x_2 - \hat{x}_2),$$

$$\dot{\hat{x}}_3 = \{K_{31}\cdot f(N)\}\mathrm{sign}(x_1 - \hat{x}_1),$$

$$\dot{\hat{x}}_4 = \{K_{42}\cdot f(N)\}\mathrm{sign}(x_2 - \hat{x}_2), \tag{3}$$

where x_1 is the line current difference between phases a and b; x_2 is the line current difference between phases b and c; x_3 is the line back EMF (for line ab); x_4 is the line back EMF (for line bc); symbol "$\wedge$" means estimated value of corresponding variables; $f(N)$ is the function of speed which is the ratio between actual speed to that of maximum speed; K_{11} and K_{22} are the line current observer gains; K_{31} and K_{42} are the back EMF observer gains.

Sliding surface $S = \begin{pmatrix} x_1 - \hat{x}_1 \\ x_2 - \hat{x}_2 \end{pmatrix}$ and the tracking error is defined as $e = x - \hat{x}$. Hence, the error dynamics for Eq. (3) can be written as

$$\dot{e}_1 = -\frac{1}{L}e_3 - K_{11}\mathrm{sign}(e_1),$$

$$\dot{e}_2 = -\frac{1}{L}e_4 - K_{22}\mathrm{sign}(e_2),$$

$$\dot{e}_3 = -\Big(K_{31}\cdot f(N)\Big)\mathrm{sign}(e_1),$$

$$\dot{e}_4 = -\Big(K_{42}\cdot f(N)\Big)\mathrm{sign}(e_2). \tag{4}$$

The candidate Lyapunov function is defined as

$$v(e) = \frac{1}{2}e_2^2 + \frac{1}{2}e_2^2.$$

The time derivative of $v(e)$ is calculated as

$$\dot{v}(e) = e_1\dot{e}_1 + e_2\dot{e}_2$$

$$= e_1\left(-\frac{1}{L}e_3 - K_{11}\mathrm{sign}(e_1)\right)$$

$$+ e_2\left(-\frac{1}{L}e_4 - K_{22}\mathrm{sign}(e_2)\right).$$

To force the asymptotic convergence of the error to zero ($\dot{v}(e)<0$), this limits the observer gain as

- If $e_1 > 0$, the switching gain $K_{11} > -\frac{1}{L}e_3$;
- If $e_1 < 0$, the switching gain $K_{11} > \frac{1}{L}e_3$;
- if $e_2 > 0$, the switching gain $K_{22} > -\frac{1}{L}e_4$;
- if $e_2 < 0$, the switching gain $K_{22} > \frac{1}{L}e_4$.

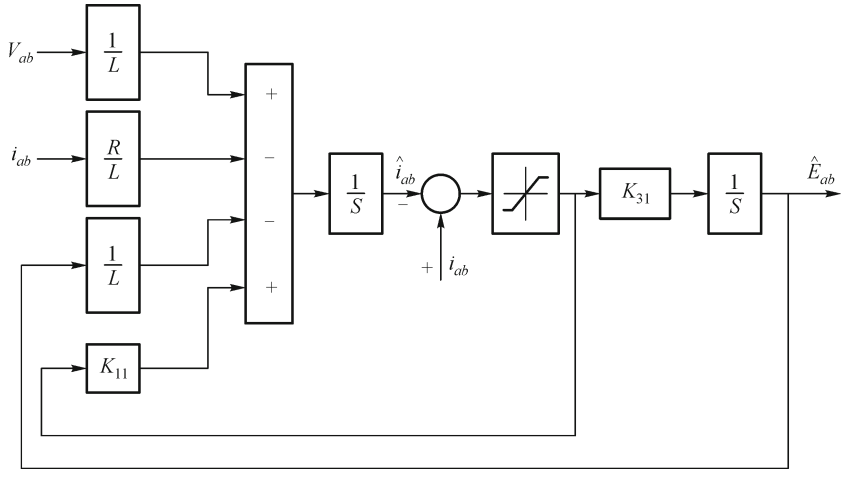

Fig. 2 Conventional sliding mode observer

Hence, from above discussion, the observer gain value is chosen in such a way that $K_{11} > \frac{1}{L}|e_3|$ and $K_{22} > \frac{1}{L}|e_4|$ to make $v(e)$ a globally asymptotically stable [24] function.

In order to constrain the system to work in the sliding surface S, $e_1(t) = e_2(t) = 0$ which leads to

$$\frac{1}{L}e_3 = -K_{11}\text{sign}(e_1),$$

$$\frac{1}{L}e_4 = -K_{22}\text{sign}(e_2).$$

.

The reduced order sliding mode is governed by

$$\dot{e}_3 = \frac{K_{31} \cdot f(N)}{L \cdot K_{11}}e_3,$$

$$\dot{e}_4 = \frac{K_{42} \cdot f(N)}{L \cdot K_{22}}e_4.$$

By these assumptions the tracking error converges to zero exponentially. According to the sliding mode observer design as proposed in Ref. [24], the main controller parameters affecting the controller performance are K_{31} and K_{11}. Among these parameters, back EMF observer gain (K_{31}) is tuned to obtain actual rotor position in the proposed method. As the back EMF is a function of speed, the observer gain is made to increase with increase in speed, in the proposed method. Hence, K_{31} is designed and the job of fine tuning in the estimated position is left to the function of speed as shown in Fig. 3. With the inclusion of speed component, the observer gain automatically gets adjusted from zero to a required value rapidly and suitably for various ranges of speeds.

4 Results and discussion

The overall system block diagram of the proposed sensorless drive is shown in Fig. 4. The experimental setup consists of a 1.2 HP, 3000 rpm, four-pole BLDC motor and LEMs (sensors currents and terminal voltages). The entire drive system is controlled by a DSP TMS320LF2407A. Table 1 shows the specifications of the BLDC motor.

Table 1 BLDC motor parameters

parameter	symbol	value
resistance	R_s	5.25 Ω
inductance	L_s	21 mH
back EMF constant	λ_f	0.34 V/rpm
moment of inertia	J	0.00012 kg·m^2
viscous damping coefficient	B	0.00006 N·m/(rad/sec)
nominal voltage	V_n	380 V
nominal frequency	F_n	50 Hz

Experimental and simulation results of the conventional sliding mode observer are depicted in Figs. 5, 6, and 7.

The top trace of Figs. 5, 6, and 7 shows the trapezoidal line back EMF, the second trace shows the rotor position produced from estimated back EMF, the third trace depicts the rotor position through the position sensor placed on the shaft of the motor, and the bottom trace depicts the speed of the motor.

CASE 1 Performance of the sliding mode observer with observer gain designed for low speed (K_{31} = 25)

The motor is made to operate for a wide range of speed by selecting the observer gain for lower speeds. With current observer gain (K_{11}, K_{22}) being determined as in Ref. [24], the second step is to determine back EMF gains K_{31} and K_{42}, which are maintained as a low value to estimate the rotor position. This estimated rotor position from conventional method suits only for low range of speeds which is depicted in Fig. 5(b). Based on the theory of sliding mode

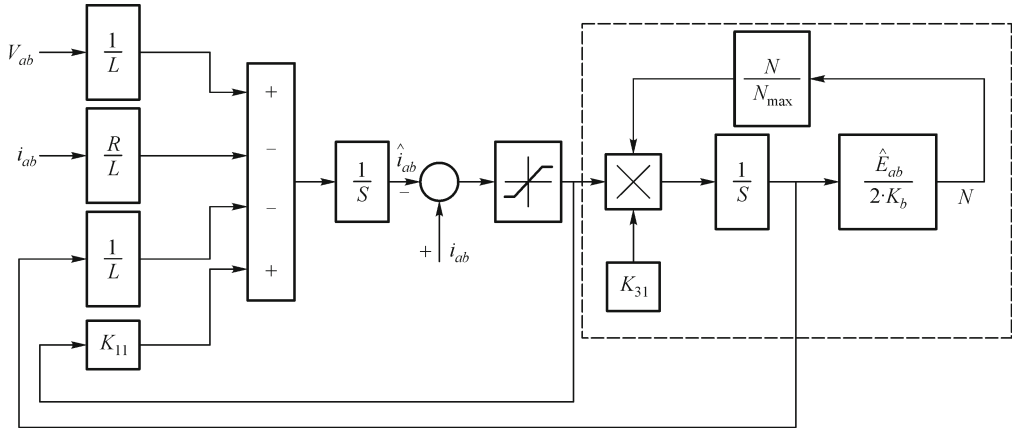

Fig. 3 The proposed sliding mode observer

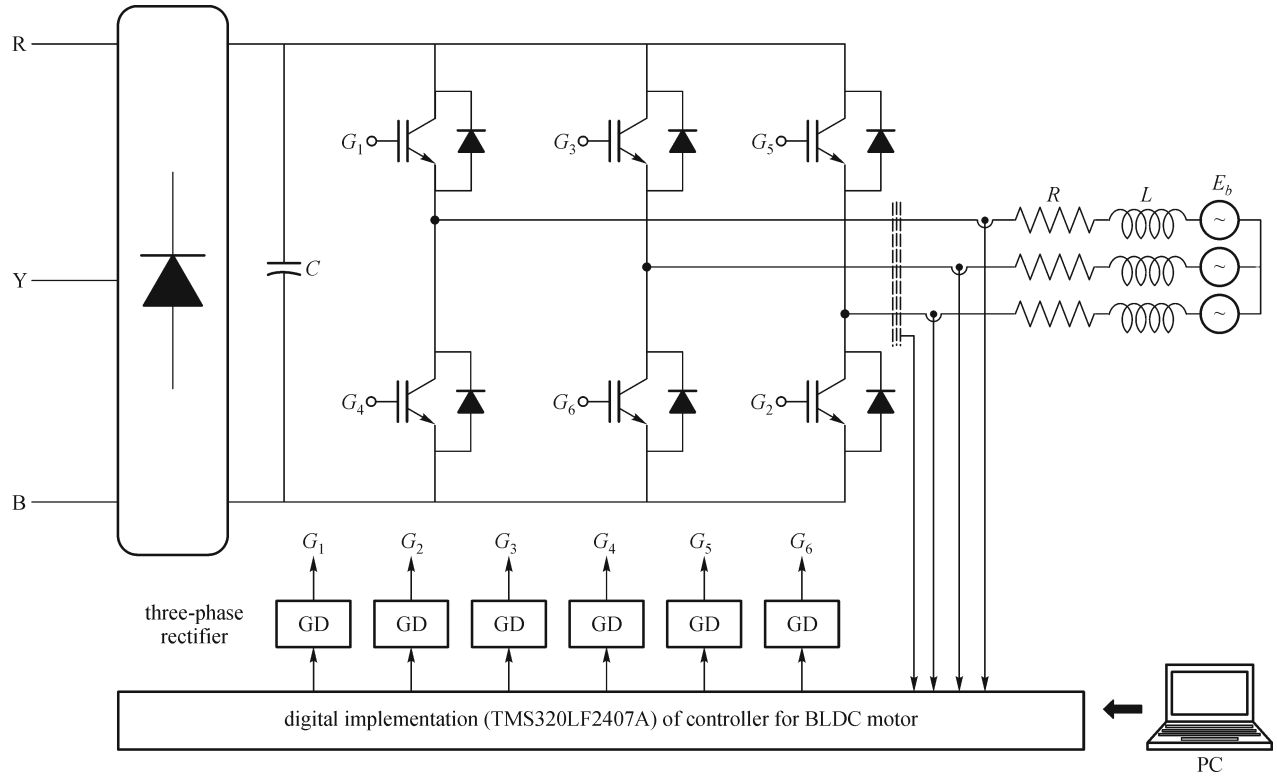

Fig. 4 Block diagram of the experimental set-up

observer, smaller observer gains (K_{31}, K_{42}) as given in this case stand a stronger risk of losing observation convergence for higher speeds. This introduces a phase shift of about 19° for a speed of 1500 rpm as depicted in Fig. 5(d). This phase shift increases up to 26° for a speed of 2500 rpm which is depicted in Fig. 5(f). This observation error appears unacceptably large at larger speeds which indicate the failure of the sliding mode observer over decreased back EMF observer gain. The validity of the conventional observer structure is verified by simulation and the results are given in Figs. 5(a), 5(c), and 5(e). It is seen from Fig. 5(a) that the precision focusing and tracking of the rotor position are well performed while the motor is made to run under low speed. When the same observer gain is made to operate for a speed of 1500 rpm, it contains a positional error of about 18° lag compared to the actual rotor position as depicted in Fig. 5(c). Figure 5(e) depicts the simulated system observation error for a speed of 2500 rpm having a positional error of 36° lag with respect to the actual rotor position.

CASE 2 Performance of the sliding mode observer with observer gain designed for medium speed (K_{31} = 75)

The performance of the motor operating from low speed to high speed, by tuning the observer gain for a medium range of speed is evaluated. With a medium sliding mode observer gain, the estimated rotor position produces a phase shift of about 17° for a speed of 2500 rpm as shown in the second trace of Fig. 6(f) and the phase delay increases with increase in speed. The same observer gain value produces undesired switching near the zero crossing of the estimated back EMF for a speed of 500 rpm which is depicted in Fig. 6(b) and these unwanted switching increases with decrease in speed. Since the observer gain is selected for medium speed the estimation error becomes zero and synchronizes with the actual back EMF for a speed of 1500 rpm as depicted in Fig. 6(d). The simulation results for the above mentioned conventional observer are shown in Figs. 6(a), 6(c), and 6(e). In Fig. 6(a) it is to be noticed that the estimated rotor position consists of unwanted switching compared to the actual position for a speed of 500 rpm. With the same observer gain the rotor position is accurately tracked without any error for a speed of 1500 rpm which is depicted in Fig. 6(c). The estimated rotor position has a phase shift of 18° with respect to actual for a speed of 2500 rpm as shown in the second and third trace of Fig. 6(e).

CASE 3 Performance of the sliding mode observer with observer gain designed for high speed (K_{31} = 125)

The motor is operated from low speed to high speed, by tuning the observer gain for higher speeds. With a high sliding mode observer gain, the actual rotor position perfectly matches with the estimated for a large range of

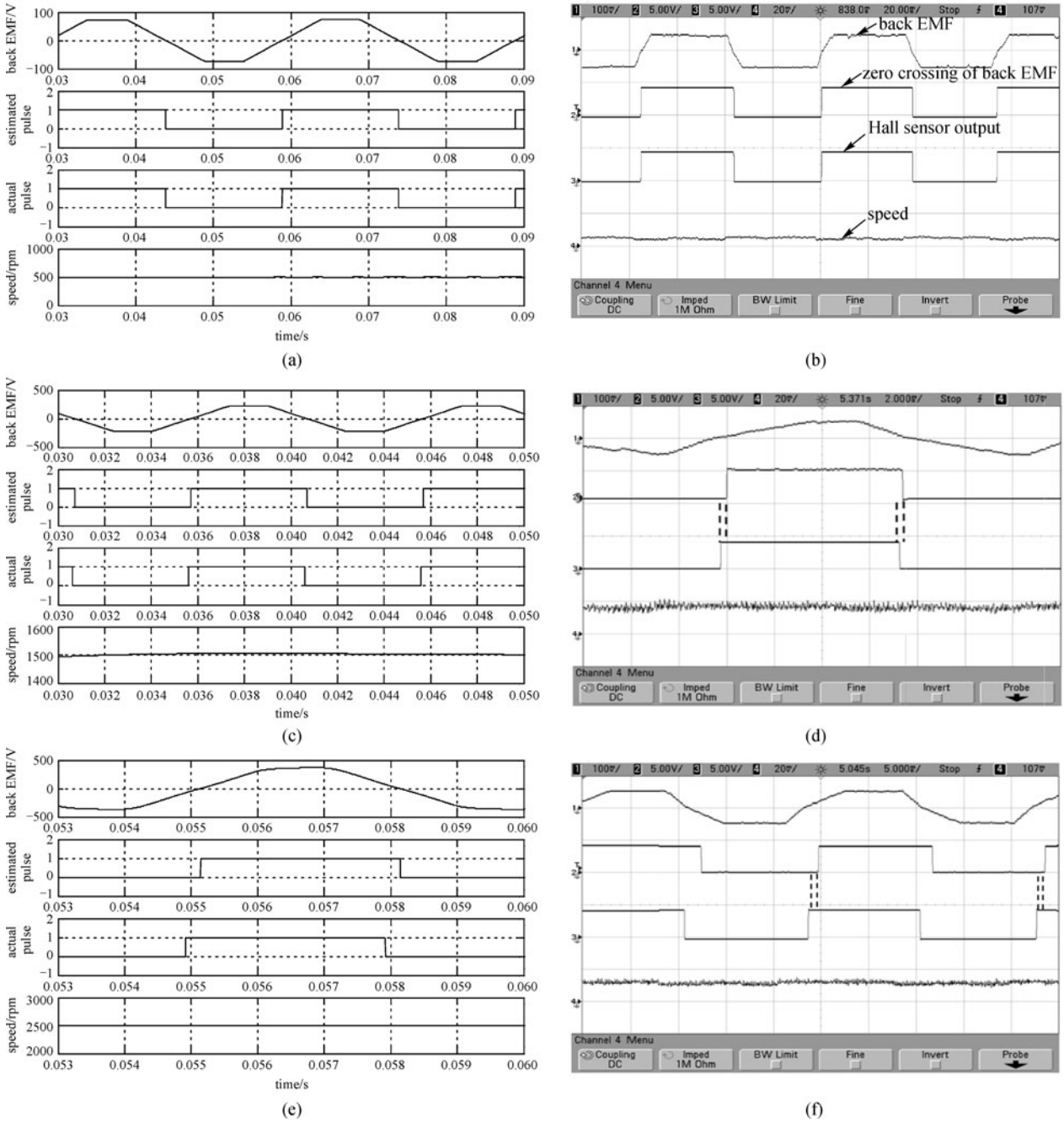

Fig. 5 Sliding mode observer with low observer gain (K_{31} = 25). (a) Simulation result at low speed (N = 500 rpm); (b) experimental result at low speed (N = 500 rpm); (c) simulation result at medium speed (N = 1500 rpm); (d) experimental result at medium speed (N = 1500 rpm); (e) simulation result at high speed (N = 2500 rpm); (f) experimental result at high speed (N = 2500 rpm) (y-axis: back EMF, 200 mV/div; zero crossing of back EMF: 5 V/div; Hall sensor output: 5 V/div; speed: 20 mV/div; x-axis: time, 0.02 s/div)

speed which is shown in Fig. 7(f) and produces undesired switching near the zero crossing of the estimated back EMF for a speed of 1500 rpm which is depicted in Fig. 7(d). This unwanted switching increases with decrease in speed which is depicted for a speed of 500 rpm in Fig. 7(b). The undesired switching in the estimated position leads to the introduction of unreliable states during the rotation of the motor. The validity of the conventional observer structure is verified by the simulation and the results are given in Figs. 7(a), 7(c), and 7(e). In Fig. 7(a), the estimated rotor position containing the unwanted switching due to high observer gain is shown. Figure 7(c) shows that the number of unwanted switching decreased for a speed of 1500 rpm as

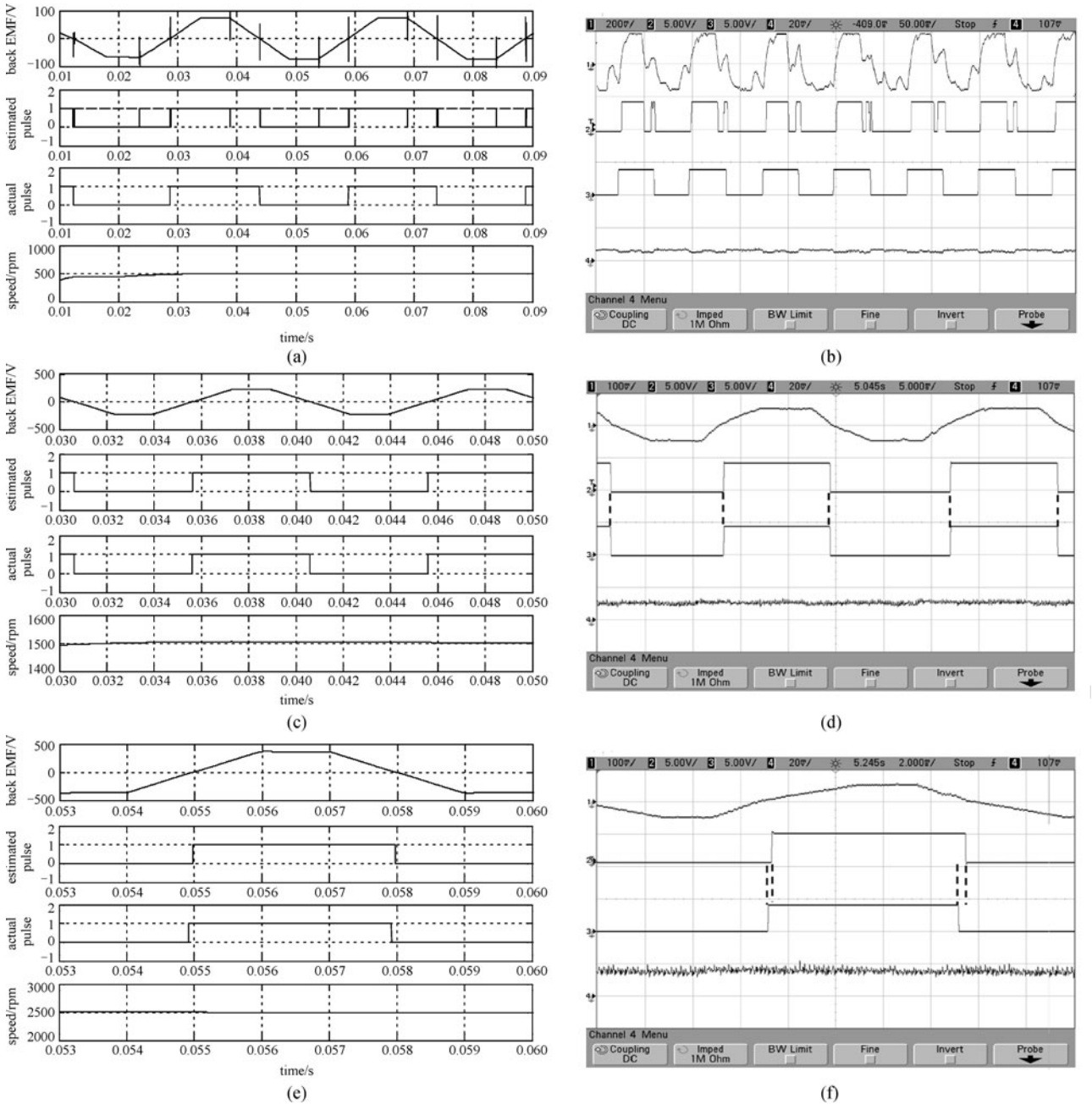

Fig. 6 Sliding mode observer with medium observer gain (K_{31} = 75). (a) Simulation result at low speed (N = 500 rpm); (b) experimental result at low speed (N = 500 rpm); (c) simulation result at medium speed (N = 1500 rpm); (d) experimental result at medium speed (N = 1500 rpm); (e) simulation result at high speed (N = 2500 rpm); (f) experimental result at high speed (N = 2500 rpm) (y-axis: back EMF, 200 mV/div; zero crossing of back EMF: 5 V/div; Hall sensor output: 5 V/div; speed: 20 mV/div; x-axis: time, 0.02 s/div)

compared to that of low speed. It is also seen from Fig. 7(e) that the conventional sliding mode observer has achieved a fast observation in estimating with low observation error for a speed of 2500 rpm.

From the above discussion, it can be seen that the unaltered back EMF observer gain works well only for its designed range of speeds. To eliminate this setback a new modified sliding mode observer is proposed, where a varying gain in accordance with variation of speed is included to estimate the rotor position of the motor without any hindrance.

- Performance of the proposed sliding mode observer

Experimental results of the proposed sliding mode observer are depicted in Fig. 8. The top trace shows the

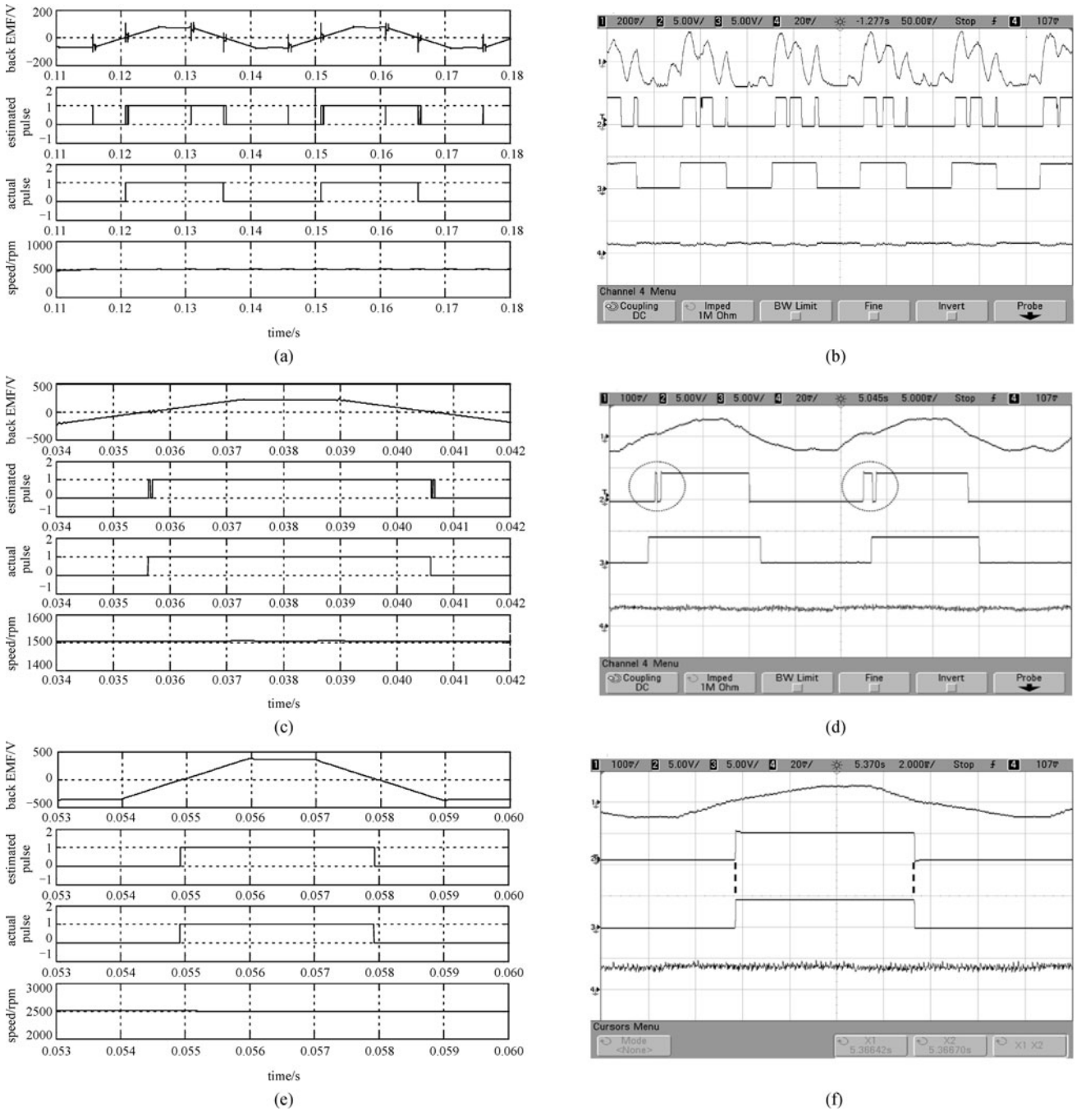

Fig. 7 Sliding mode observer with high observer gain (K_{31} = 125). (a) Simulation result at low speed (N = 500 rpm); (b) experimental result at low speed (N = 500 rpm); (c) simulation result at medium speed (N = 1500 rpm); (d) experimental result at medium speed (N = 1500 rpm); (e) simulation result at high speed (N = 2500 rpm); (f) experimental result at high speed (N = 2500 rpm) (y-axis: back EMF, 200 mV/div; zero crossing of back EMF: 5 V/div; Hall sensor output: 5 V/div; speed: 20 mV/div; x-axis: time, 0.02 s/div)

trapezoidal line back EMF, the second trace shows the rotor position produced from estimated back EMF, the third trace depicts the rotor position through the position sensor placed on the shaft of motor, and the bottom trace depicts the speed of the motor.

The motor is made to operate from low speed to high speed with the proposed method to verify the dynamics of the observer as shown in Fig. 8(a). Figures 8(b), 8(c), and 8(d) show the expanded view for lower, medium, and higher speeds, respectively. Figure 8(b) illustrates that the proposed sliding mode observer suits for low speed without any undesired switching near zero crossing of the estimated back EMF, Fig. 8(c) shows that the estimated rotor position matches with the actual rotor position for

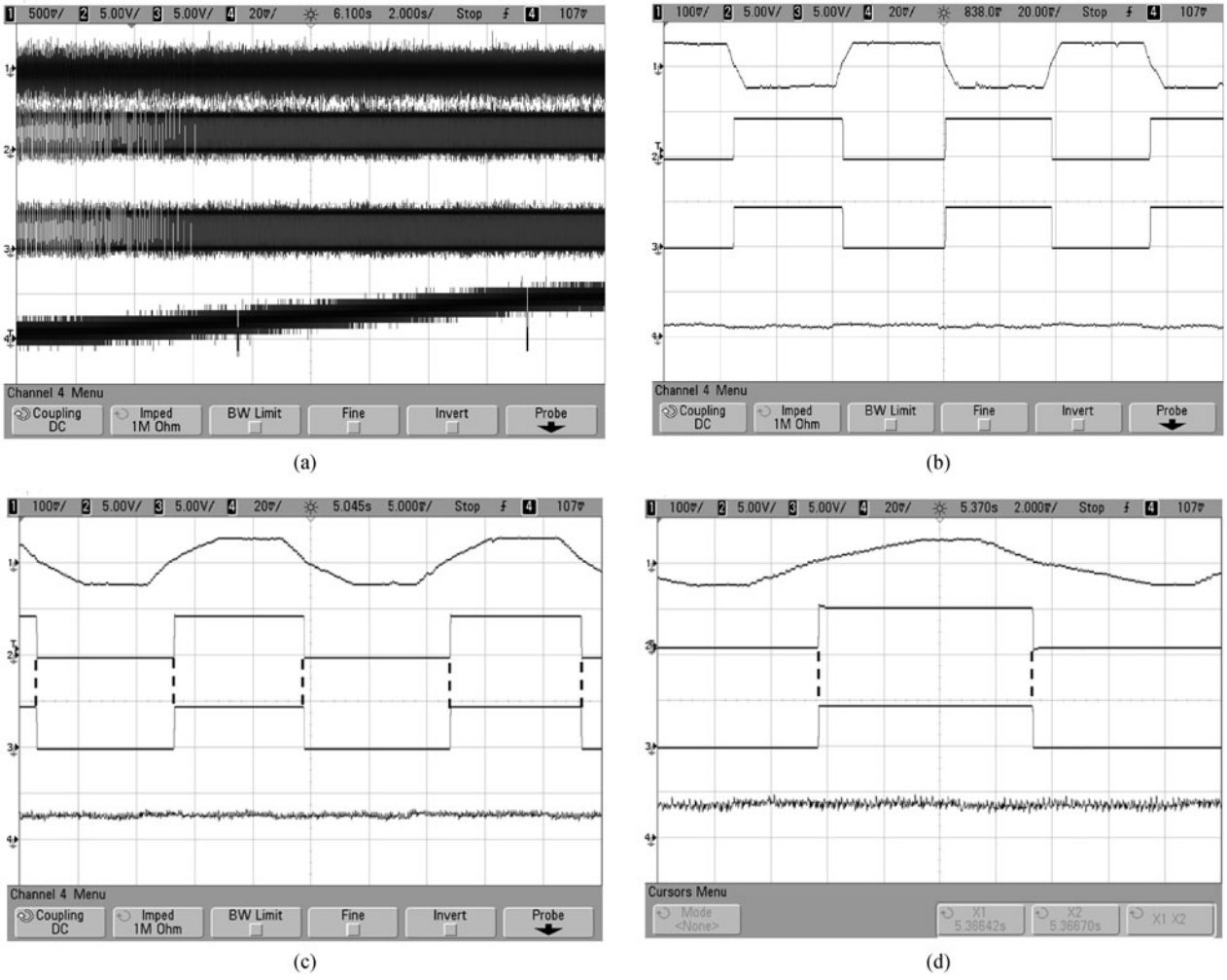

Fig. 8 Experimental results of the proposed method (K_{31} = 150). (a) Variation of speed from low speed (N = 500 rpm) to high speed (N = 2500 rpm); (b) performance of proposed method under low speed (N = 500 rpm); (c) performance of proposed method under medium speed (N = 1500 rpm); (d) performance of proposed method under high speed (N = 2500 rpm) (y-axis: back EMF, 200 mV/div; zero crossing of back EMF: 5 V/div; Hall sensor output: 5 V/div; speed: 20 mV/div; x-axis: time, 0.02 s/div)

medium speed, and Fig. 8(d) depicts the synchronization of estimated rotor position with the actual rotor position without any phase delay. The estimated rotor position is validated with the actual Hall sensor output which is presented in the third trace of Figs. 8(a), 8(b), 8(c), and 8(d).

5 Conclusions

In this paper, the back EMF is estimated indirectly with the help of estimated and actual line currents through modified sliding mode observer. This estimated back EMF in turn interprets the rotor position through the zero crossing points. Inclusion of speed as a function in the observer gain of sliding mode observer eliminates the multiple zero crossing at low speeds and avoids mismatch between the estimated and actual back EMFs at higher speeds. Simulation and experimental results have confirmed the good convergence and robust performance of the observer.

Acknowledgements This work has been carried out in the Power Converters Research Laboratory, EEE Department NIT, Trichy. The authors are grateful to the administration of NIT Trichy and to the National Mission on Power Electronics Technology (NaMPET), Department of Information Technology, and Government of India for the financial aid towards infrastructure development of this lab.

References

1. Becerra R C, Ehsani M. High-speed torque control of brushless permanent magnet motors. IEEE Transactions on Industrial Electronics, 1988, 35(3): 402–406
2. Hubik V, Sveda M, Singule V. On the development of BLDC motor

control run-up algorithms for aerospace application. In: Proceedings of the 13th Power Electronics and Motion Control Conference (EPE-PEMC 2008). 2008, 1620–1624

3. Becerra R C, Jahns T M, Ehsani M. Four-quadrant sensorless brushless ECM drive. In: Proceedings of the Sixth Annual Applied Power Electronics Conference and Exposition (APEC 1991). 1991, 202–209
4. Iizuka K, Uzuhashi H, Kano M, Endo T, Mohri K. Microcomputer control for sensorless brushless motor. IEEE Transactions on Industry Applications, 1985, IA-21(3): 595–601
5. Shao J, Nolan D, Hopkins T. A novel direct back EMF detection for sensorless brushless DC (BLDC) motor drives. In: Proceedings of the Seventeenth Annual IEEE Applied Power Electronics Conference and Exposition (APEC 2002). 2002, 1: 33–37
6. Su G J, McKeever J W. Low-cost sensorless control of brushless DC motors with improved speed range. IEEE Transactions on Power Electronics, 2004, 19(2): 296–302
7. Damodharan P, Sandeep R, Vasudevan K. Simple position sensorless starting method for brushless DC motor. IET Electric Power Applications, 2008, 2(1): 49–55
8. Damodharan P, Vasudevan K. Sensorless brushless DC motor drive based on the zero-crossing detection of back electromotive force (EMF) from the line voltage difference. IEEE Transactions on Energy Conversion, 2010, 25(3): 661–668
9. Ogasawara S, Akagi H. An approach to position sensorless drive for brushless DC motors. IEEE Transactions on Industry Applications, 1991, 27(5): 928–933
10. Jahns T M, Becerra R C, Ehsani M. Integrated current regulation for a brushless ECM drive. IEEE Transactions on Power Electronics, 1991, 6(1): 118–126
11. Acarnley P P, Watson J F. Review of position-sensorless operation of brushless permanent-magnet machines. IEEE Transactions on Industrial Electronics, 2006, 53(2): 352–362
12. Kim T, Lee H W, Ehsani M. Position sensorless brushless DC motor/generator drives: Review and future trends. IET Electric Power Applications, 2007, 1(4): 557–564
13. Zhang L, Xiao W, Qu W. Sensorless control of BLDC motors using an improved low-cost back EMF detection method. In: Proceedings of the 2006 IEEE Power Electronics Specialists Conference. 2006, 322–328
14. Moreira J C. Indirect sensing for rotor flux position of permanent magnet AC motors operating over a wide speed range. IEEE Transactions on Industry Applications, 1996, 32(6): 1394–1401
15. Shen J X, Zhu Z Q, Howe D. Sensorless flux-weakening control of permanent-magnet brushless machines using third harmonic back EMF. IEEE Transactions on Industry Applications, 2004, 40(6): 1629–1636
16. Shen J X, Iwasaki S. Sensorless control of ultrahigh-speed PM brushless motor using PLL and third harmonic back EMF. IEEE Transactions on Industrial Electronics, 2006, 53(2): 421–428
17. Johnson J P, Ehsani M, Guzelgunler Y. Review of sensorless methods for brushless DC. In: Proceedings of the 1999 IEEE Industry Applications Conference (The Thirty-Fourth IAS Annual Meeting). 1999, 1: 143–150
18. Dhaouadi R, Mohan N, Norum L. Design and implementation of an extended Kalman filter for the state estimation of a permanent magnet synchronous motor. IEEE Transactions on Power Electronics, 1991, 6(3): 491–497
19. Qiu A, Wu B, Kojori H. Sensorless control of permanent magnet synchronous motor using extended Kalman filter. In: Proceedings of the Canadian Conference on Electrical and Computer Engineering (CCECE 2004). 2004, 3: 1557–1562
20. Peixoto Z M A, Freitas Sa F M, Seixas P F, Menezes B R, Cortizo P C, Lacerda W S. An interior permanent magnet synchronous motor position control using sliding mode. In: Proceedings of the 1995 International Conference on Power Electronics and Drive Systems (PEDS 95). 1995, 599–604
21. Kim Y S, Ahn J Y, You W S, Cho K M. A speed sensorless vector control for brushless DC motor using binary observer. In: Proceedings of the 1996 IEEE IECON 22nd International Conference on Industrial Electronics, Control, and Instrumentation. 1996, 3: 1746–1751
22. Feyzi M R, Shafiei M, Koushahi M B, Mozaffari Niapour S A K. Position sensorless direct torque control of brushless DC drives based on sliding mode observer using NSGA-II algorithm optimization. In: Proceedings of the 2011 2nd Power Electronics, Drive Systems and Technologies Conference (PEDSTC). 2011, 151–156
23. Fakham H, Djemai M, Reama A, Blazevic P. Sliding mode observer for position and speed estimations in brushless DC motor (BLDCM). In: Proceedings of the 2004 IEEE International Conference on Industrical Technology (IEEE ICIT'04). 2004, 1: 121–126
24. Fakham H, Djemai M, Busawon K. Design and practical implementation of a back-EMF sliding-mode observer for a brushless DC motor. IET Electric Power Applications, 2008, 2(6): 353–361
25. Deenadayalan A, Saravana Ilango G. Modified sliding mode observer for position and speed estimations in brushless DC motor. In: Proceedings of the 2011 Annual IEEE India Conference (INDICON). 2011, 1–4